Precipitation Conditions in Offshore Wind Farm Zones

Insights from Satellites and Weather Simulations

Ivanova, Tsvetelina; Palatos-Plexidas, Alexandros; Porchetta, Sara; Buckingham, Sophia; Beeck, Jeroen Van; Cruz, Lesley De; Helsen, Jan; Munters, Wim

DOI
10.1088/1742-6596/3131/1/012005

Publication date
2025

Document Version
Final published version

Published in
Journal of Physics: Conference Series

Citation (APA)
Ivanova, T., Palatos-Plexidas, A., Porchetta, S., Buckingham, S., Beeck, J. V., Cruz, L. D., Helsen, J., & Munters, W. (2025). Precipitation Conditions in Offshore Wind Farm Zones: Insights from Satellites and Weather Simulations. *Journal of Physics: Conference Series*, *3131*(1), Article 012005. https://doi.org/10.1088/1742-6596/3131/1/012005

Journal of Physics:
Conference Series

PAPER • **OPEN ACCESS**

Precipitation Conditions in Offshore Wind Farm Zones: Insights from Satellites and Weather Simulations

To cite this article: Tsvetelina Ivanova *et al* 2025 *J. Phys.: Conf. Ser.* **3131** 012005

Journal of Physics: Conference Series **3131** (2025) 012005 doi:10.1088/1742-6596/3131/1/012005

Precipitation Conditions in Offshore Wind Farm Zones: Insights from Satellites and Weather Simulations

Tsvetelina Ivanova[1,2], Alexandros Palatos-Plexidas[1,3], Sara Porchetta[4], Sophia Buckingham[5], Jeroen van Beeck[1], Lesley De Cruz[3,6], Jan Helsen[2], Wim Munters[1]

[1] Environmental and Applied Fluid Dynamics Department, von Karman Institute, Chaussée de Waterloo 72, 1640 Rhode-Saint-Genèse, Belgium
[2] Department of Engineering Technology, Vrije Universiteit Brussel, Pleinlaan 2, 1050 Brussels, Belgium
[3] Electronics and Informatics Department, Vrije Universiteit Brussel, Pleinlaan 9, 1050 Brussels, Belgium
[4] Faculty of Civil Engineering and Geosciences, Delft University of Technology, Stevinweg 1, 2628 CN Delft, The Netherlands
[5] Research & Innovation ENGIE Laborelec, 1630 Linkebeek, Belgium
[6] Royal Meteorological Institute of Belgium, 1180 Brussels, Belgium

E-mail: tsvetelina.ivanova@vki.ac.be

Abstract. Characterizing wind and precipitation conditions is essential for the durability and maintenance of wind turbine components. Precipitation-driven leading edge erosion of turbine blades has emerged as a significant concern, as it compromises aerodynamic performance and shortens blade lifespan. This study investigates wind and precipitation patterns across a large region of Europe, with a particular focus on the Southern Bight of the North Sea. Using ten years of ERA5 atmospheric reanalysis data, we analyze wind and precipitation conditions, and derive an erosion risk map based on the combined effects of precipitation and blade tip speed. To capture local-scale variability, we employ high-resolution WRF simulations over a three-year period to downscale ERA5 data for the Southern Bight region. These simulations are used to generate detailed seasonal maps of wind speed, precipitation, and erosion risk on a 3 km grid. Additionally, we compare precipitation estimates from ERA5, as well as from NASA's IMERG satellite product, NORA3 hindcast archive, and from the WRF model output against three Belgian weather stations. We emphasize the added value of high-resolution modeling in capturing precipitation heterogeneity that influences blade erosion rates. Integrating both large-scale and regional weather data supports site screening in early-stage wind farm planning, material selection in blade coatings, and maintenance prioritization, especially offshore, thus contributing to the cost-effectiveness of wind energy projects.

1 Introduction

As the global demand for clean energy increases, offshore wind farms have become central to achieving renewable energy targets. The reliability and longevity of wind turbine blades depends significantly on their ability to withstand environmental stressors, particularly in offshore environments where in-situ measurements are scarce due to logistical challenges. A key blade degradation mechanism is precipitation-driven leading-edge erosion (LEE), which compromises aerodynamic performance, reduces energy yield, and increases maintenance costs. LEE has received growing attention in recent years. Early studies demonstrated how erosion degrades blade efficiency and structural integrity [1], while others highlighted the limitations of protective coatings and the need for improved materials [2]. Mitigation strategies such as reducing tip speed during intense rainfall have shown promise in extending blade lifetimes [3, 4, 5]. The concurrence of high wind speeds and intense precipitation has been identified as a key factor in erosion progression [6]. Understanding the meteorological conditions that drive LEE has become a central research focus. Several studies have investigated the influence of extreme precipitation events, using radar-derived climatologies [7] and offshore precipitation assessments [8] to characterize rain-induced surface wear. Numerical weather prediction models have further advanced this understanding by simulating the effects of precipitation type and intensity – particularly convective and mixed-phase events – on erosion potential [9]. Complementing these efforts, observational studies have produced rainfall maps and translated them into monthly blade mass loss estimates [10]. Satellite-based precipitation products have also been leveraged to assess long-term erosion risks and estimate blade lifetimes across broader spatial scales [11]. A comprehensive review of atmospheric drivers [12] reinforces the importance of wind speed and precipitation intensity as primary contributors to LEE.

Recent advances include data-driven frameworks that combine blade inspection records with mesoscale weather simulations to improve damage prediction accuracy [13]. Erosion onset times are mapped in regions such as Scandinavia, offering finer-scale perspectives on spatial variability [14], while disdrometer-based analyses have emphasized the role of raindrop size and liquid water content [15]. Erosion atlases have been developed for Dutch offshore, coastal, and onshore environments [16, 17]. The reliability of satellite-derived precipitation data has also been evaluated in complex terrain to assess its suitability for erosion modeling [18].

The present study enriches existing research by quantifying the risk of erosion in offshore wind farms through a combination of global reanalysis data, satellite-based precipitation retrievals, and regional downscaling over the Southern Bight of the North Sea via numerical weather prediction models. Specifically, we use the ERA5 reanalysis dataset from the European Centre for Medium-Range Weather Forecasts (ECMWF) [19], NASA's IMERG product (Integrated Multi-satellitE Retrievals for Global Precipitation Measurement v07) [20, 21], and three years of simulations with the Weather Research and Forecasting (WRF) model [22, 23]. For verification purposes, we evaluate all datasets against precipitation measurements from three Belgian weather stations [24, 25] and the 3-km Norwegian reanalysis dataset (NORA3) [26, 27], extracted at these weather station locations. Finally, we produce high-resolution seasonal wind and precipitation maps based on WRF output and derive a seasonal erosion risk map by incorporating hourly precipitation and blade tip speeds. These results support informed decisions on protective coatings, maintenance prioritization, and the implementation of erosion-safe operational strategies.

The structure of the paper is as follows: Section 2 presents the methodology, Section 3 covers a large-scale analysis of ERA5, Section 4 compares the datasets to weather station observations and discusses regional insights in the Southern Bight of the North Sea using WRF, and Section 5 concludes the paper.

2 Method and data

This study analyzes precipitation and wind conditions using three datasets: atmospheric reanalysis ERA5, satellite-based IMERG, and high-resolution WRF simulations. The period of interest for the ERA5 and IMERG datasets is 10 years (2014-2023) over a selected domain spanning latitudes 36°N to 71°N and longitudes 15°W to 30°E, as shown in Figure 1a. This region encompasses much of Europe with an active offshore wind farm development. The WRF simulations cover 3 years (2021, 2022, 2023), and they are performed over a nested domain setup, see Figure 1b. The wind farm locations shown in the figures are obtained from [28] and [29].

Each of the three datasets offers its advantages. ERA5 and IMERG provide long-term historical records, enabling climatological assessments at relatively low computational cost, while WRF simulations offer high-resolution insights into localized weather conditions. Unlike ERA5 and IMERG, which are retrospective, WRF can also be used for forecasting. However, WRF is also valuable for long-term high-resolution wind resource assessments. In this study, we analyze total precipitation and 100-m wind speed from ERA5, daily accumulated precipitation from IMERGDFv07, as well as precipitation and wind speed from WRF simulations. We compare these datasets to three Belgian weather stations (for the 3-year-

period of WRF simulations). Additionally, we include a comparison with NORA3 data at these three stations.

2.1 LEE risk indicator

To evaluate the potential for rain-induced damage to wind turbine blades, we introduce an erosion risk indicator. This simple metric provides a meteorological perspective on the influence of wind speed and precipitation, emphasizing regions where their concurrence may accelerate blade erosion without taking into account material properties. The risk indicator uses hourly wind speed and precipitation data as inputs, as these two atmospheric variables are key drivers for leading edge erosion. By relying on available meteorological datasets, the indicator offers a practical tool for early-stage site assessment and maintenance planning. The LEE risk indicator is based on the tip speed of the turbine blades, which is obtained from the hourly wind speed values using a standard wind turbine power curve from the IEA 10MW reference wind turbine [30] with a tip-speed ratio of 7. For wind speeds below the cut-in threshold (4 $\mathrm{m\,s^{-1}}$) or above the cut-out threshold (25 $\mathrm{m\,s^{-1}}$), the turbine does not operate, and the tip speed is zero. Between the cut-in and rated wind speeds, the tip speed increases linearly with wind speed, while for wind speeds beyond the rated threshold (11 $\mathrm{m\,s^{-1}}$), the tip speed remains constant at its maximum operational value. The tip speed is then used in the erosion risk computation.

The LEE risk indicator $I(x, y)$ is computed as the product of hourly precipitation $P(t, x, y)$ and blade tip speed $U_{\mathrm{tip}}(t, x, y)$ at each grid point and time. This product is then averaged over time to obtain a mean at each location. To facilitate spatial comparison across regions with different environmental baselines, the result is normalized by the product of the domain-averaged temporal means of precipitation and tip speed:

$$I(x, y) = \frac{\langle P(t, x, y) \cdot U_{\mathrm{tip}}(t, x, y) \rangle_t}{\langle P(t, x, y) \rangle_t^{\mathrm{domain}} \cdot \langle U_{\mathrm{tip}}(t, x, y) \rangle_t^{\mathrm{domain}}},$$

where $\langle \cdot \rangle_t$ denotes the temporal average over a selected period (e.g. seasonal or multi-year), and $\langle \cdot \rangle_t^{\mathrm{domain}}$ represents the spatial average of the temporal mean across the entire domain.

2.2 IMERG precipitation dataset

The Integrated Multi-satellitE Retrievals for GPM (IMERG) dataset provides global precipitation estimates by integrating data from multiple passive microwave sensors from the Global Precipitation Measurement (GPM) constellation [20]. The dataset used in this study is the IMERG Final Daily product (GPM IMERG Final Precipitation L3 1 day 0.1° x 0.1° V07) [21]. This dataset has a spatial grid of approximately 11 km and a temporal resolution of 1 day, which indicates the total accumulated precipitation in one day (units mm/day).

IMERG's performance near coastlines is affected by the transition between land and ocean retrieval regimes and the mixed surface emissivity in these areas, which can introduce retrieval artifacts [31]. These artifacts often result in an overestimation of light precipitation and an underestimation of short-duration, high-intensity convective events, especially in flat coastal regions where ground-based validation is limited. Additionally, seasonal biases have been reported, with IMERG tending to overestimate precipitation during summer and underestimate it in winter [31].

2.3 ERA5 atmospheric reanalysis product

ERA5 is a global atmospheric reanalysis dataset produced by the ECMWF [19]. It combines numerical weather model output with observations to generate a physically consistent representation of past atmospheric conditions. ERA5 provides hourly estimates of various meteorological variables on a 0.25°×0.25° grid, which corresponds to an approximate horizontal resolution of 30 km. In this study, we analyze total precipitation and 100-m wind speed from ERA5 to assess regional wind and precipitation trends over wind farm zones.

2.4 WRF simulations

The WRF model [22, 23] version 4.5.1, `https://github.com/wrf-model/WRF/releases/tag/v4.5.1` (last accessed: 3 June 2025) is used for regional downscaling from the global ERA5 dataset. The performed simulations are over a nested domain setup, focusing on the Southern Bight of the North Sea. The outer domain (D01) has a horizontal spacing of 9 km (220×220 grid cells), while the inner domain (D02) is refined to 3 km (265×283 grid cells). The domains are shown in Figure 1b. One-way nesting is applied, and a Lambert conformal projection is used.

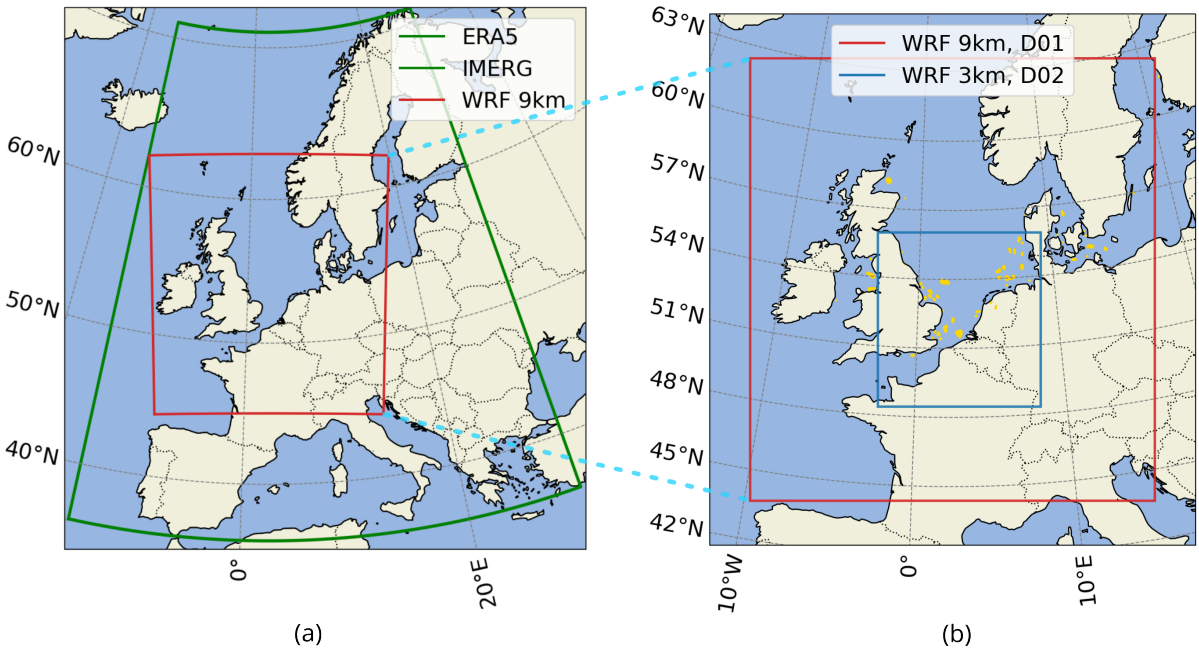

Figure 1: Data analysis regions: (a) Selected domain of interest for ERA5 and IMERG. Both datasets are on rectilinear grids with horizontal resolutions of 0.25°×0.25° and 0.1°×0.1°, respectively. (b) WRF nested domains, using a curvilinear grid with horizontal spacing of 9 km for the outer domain D01, and 3 km for the inner domain D02. Wind farm locations are marked in yellow.

Initial and boundary conditions are provided by ERA5 reanalysis data at an hourly basis. The simulations are conducted in week-long batches, covering a three-year period from 1 January 2021 to 1 January 2024, with each simulated period including a precursing 24-hour model spin-up time (that is discarded during post-processing). This three-year-long WRF dataset is generated and studied in the context of classification of wake patterns in various weather regimes [32] on an additional (higher-resolution) domain on a 1 km grid (not shown here). The WRF output analyzed in our present work is on the 3 km grid (domain D02). The variables of interest are accumulated precipitation and wind speed fields (with an hourly temporal resolution). The wind speed fields are interpolated to a typical offshore hub height of 107 m above sea level. This high-resolution output enables detailed assessments of wind and precipitation conditions at a finer grid than ERA5 and IMERG (3 km vs. 30 km and 11 km, respectively).

The WRF model setup follows established practices [33, 34, 35]. The vertical grid consists of 80 terrain-following levels, with increased resolution near the surface, and the model top is set at 50 hPa. For planetary boundary layer processes, the MYNN 2.5-level TKE scheme (option 5) is used. Cumulus parameterization (Kain-Fritsch scheme, option 1) is applied only in the outermost domain, while microphysical processes are represented using the WSM5 scheme (option 4). Radiation is handled by the RRTMG scheme (option 4) and land-surface interactions are modeled using the NOAH land surface model (option 2). Time integration is performed using a third-order Runge-Kutta scheme, and spatial advection is handled with second- to sixth-order discretization schemes. Adaptive time-stepping is applied, targeting a Courant-Friedrichs-Lewy (CFL) number of 0.6.

2.5 Belgian weather station observations

The weather station observations used for dataset intercomparison are summarized in Table 1. These observations are sourced from Meetnet Vlaamse Banken [24] and Vlaanderen Waterinfo [25]. The precipitation measurements are recorded at 10-minute intervals using tipping bucket rain gauges, with those at the Meetnet Vlaamse Banken stations manufactured by Thies Clima. To align with the temporal scales of the compared datasets in this study, we compute monthly accumulated precipitation values for each station for the three-year-long period of interest. Furthermore, to evaluate the agreement between the different datasets with weather station observations, we employ established statistical metrics [36]: corre-

Table 1: Weather observation locations in Belgium used for dataset intercomparison (2021-2023)

Location in Belgium	Label in figures	Data source	Latitude	Longitude
(near-shore) Ostend	OSTEN	Meetnet Vlaamse Banken [24]	51.238	2.930
(near-shore) Klemskerke	KLEMS	Vlaanderen Waterinfo [25]	51.225	3.008
(in-land) Lembeek	LEMBE	Vlaanderen Waterinfo [25]	50.707	4.218

lation coefficient (Corr), relative mean absolute error (rMAE), and relative bias (rBias). The correlation coefficient measures the strength and direction of the linear relationship, with values closer to 1 indicating better agreement. The rMAE quantifies the normalized mean absolute error between simulations and observations, while the rBias assesses systematic over- or underestimation.

2.6 NORA3 hindcast dataset at the Belgian weather station locations

The NORA3 dataset is a high-resolution atmospheric hindcast produced by the Norwegian Meteorological Institute. It is generated by dynamically downscaling ERA5 using the non-hydrostatic HARMONIE-AROME model at a 3 km resolution [26, 27]. In this study, we extract NORA3 precipitation data at the locations of three Belgian weather stations to compare it to the observations.

3 Large-scale analysis with ERA5

To assess the long-term spatial and temporal characteristics of precipitation and wind conditions, we analyze ERA5 over a substantial part of Europe for the selected 10 years of data, 2013-2024. Figure 2 presents maps of the multi-year averages of wind speed (a), total annual precipitation (b), and the LEE risk indicator (c), computed from hourly values of tip speed and precipitation. The maps include a selected subset of offshore wind farm zones (represented by red or gray dots) that highlight key maritime regions, including the North Sea, Baltic Sea, Celtic Sea, Norwegian Sea, North Atlantic Ocean, as well as the Black Sea and the Mediterranean Sea. This subset includes operational, approved, and early-stage wind energy projects.

The maps in Figure 2 reveal pronounced regional variations, with the highest erosion risk observed along western coasts, particularly in the Norwegian Sea and Celtic Sea. This pattern is largely driven by prevailing westerly winds that transport moisture from the Atlantic, leading to frequent precipitation and strong wind conditions – both of which contribute to accelerated blade erosion. The Baltic Sea presents a more intermediate erosion risk, where moderate precipitation levels and variable wind speeds lead to a less severe, yet still non-negligible, potential for blade degradation. In contrast, offshore wind farm zones in the Mediterranean Sea and Black Sea exhibit substantially lower erosion risks. This is primarily due to reduced precipitation in these regions, but also because of generally lower wind speed values, which result in lower tip speeds and reduced rain droplet impact forces. However, it is important to note that our analysis does not distinguish between stratiform and convective precipitation types. Convective events, which are more common in the Mediterranean region, can produce intense rainfall over short duration. These events contribute significantly to erosion due to the nonlinear relationship between droplet impact energy and material degradation. Since our indicator is based on hourly precipitation totals, it may underestimate the erosive potential of such short but intense events. Moreover, the potential role of hail is not explicitly accounted for in our risk indicator. Its inclusion in future assessments will improve the accuracy of these evaluations.

4 Regional insights in the Southern Bight of the North Sea

4.1 Comparison with weather station data in Belgium

The four datasets – ERA5 reanalysis, IMERG satellite-based estimates, NORA3 hindcast, and WRF model output – are evaluated against three weather station observations in Belgium (Table 1). Figure 3a illustrates monthly accumulated precipitation values over three years, showing that all datasets capture observed trends well, as supported by the high correlation coefficients in Figure 3b. However, a positive bias is present across all datasets when compared to station measurements in Figure 3c. The relative mean absolute errors in Figure 3d indicate that WRF with model settings from Section 2.4 exhibits the highest error magnitudes among the datasets. While NORA3 outperforms WRF in error metrics, WRF

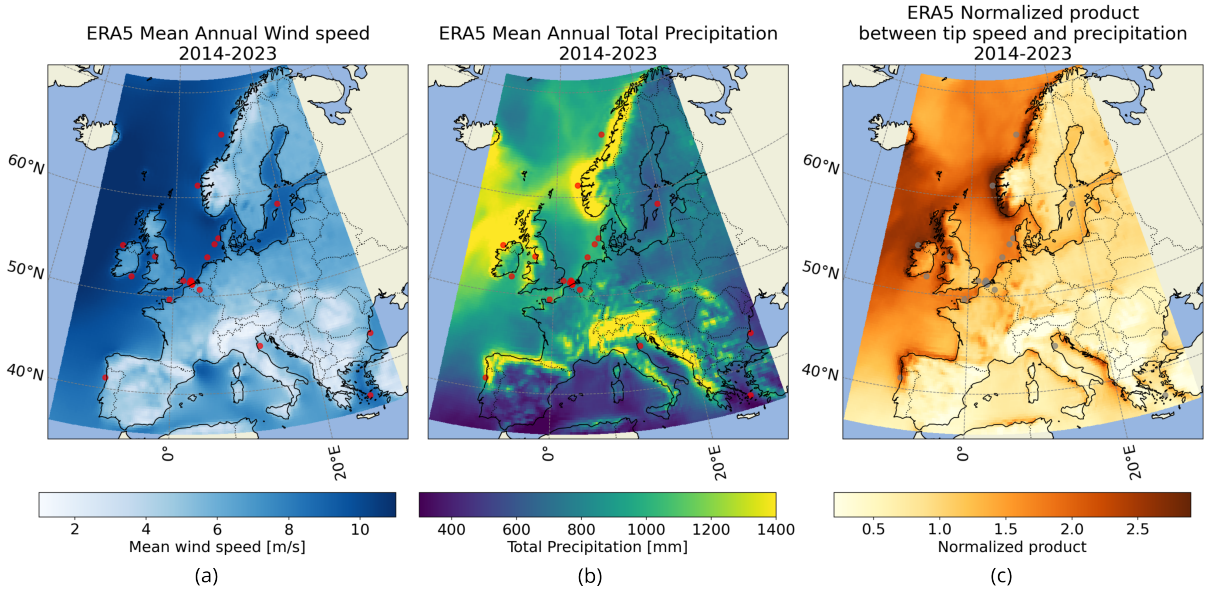

Figure 2: Averages for the period of interest (2014-2023): (a) mean wind speed, (b) mean annual precipitation, and (c) the LEE risk indicator, computed from hourly precipitation and blade tip speed over the multiple years.

demonstrates better correlation values at the two near-shore locations. Among the evaluated datasets, IMERG consistently achieves best overall performance at these weather stations.

4.2 Exploring precipitation heterogeneity

The precipitation patterns based on the three datasets over the Southern Bight of the North Sea are illustrated in Figure 4. IMERG displays pronounced differences in precipitation estimates across land, coastal, and offshore areas, particularly during spring and summer (Figure 4a). These sharp gradients along the land-sea interface are largely attributed to known limitations in the satellite retrieval algorithm, especially in regions with complex surface emissivity [31]. This discrepancy is most evident in the northeastern part of the domain where IMERG overestimates precipitation relative to ERA5 and WRF. Notably, the spatial patterns in ERA5 (Figure 4b) are preserved in the WRF downscaling (Figure 4c), indicating consistency in large-scale features.

The refined spatial resolution of WRF allows for a detailed assessment of precipitation and wind speed variations at a wind farm scale. Figure 5 presents high-resolution erosion risk assessments derived from three years of WRF simulations, revealing substantial regional and seasonal differences. Wind farms in the northeastern part of the domain – particularly those near the Dutch coast – consistently exhibit elevated erosion risks across all seasons, as seen in Figure 5c. In contrast, the southwestern part of the domain shows more localized and seasonally variable high-precipitation area, contributing to a seasonally variable erosion risk. While wind speed is generally more homogeneous across the domain with offshore values consistently higher than onshore, precipitation exhibits much greater spatial variability. This variability is the main factor shaping the seasonal LEE risk patterns. For example, in spring, the erosion risk map shows relatively uniform values, whereas in autumn – when precipitation peaks – the contrast between offshore and onshore risk becomes more pronounced. Wind farms near Belgium, the Netherlands and the eastern UK coast also show strong seasonal shifts in their associated erosion risks. In winter, despite having the highest average wind speeds, we observe a relatively moderate erosion risk due to lower precipitation totals. This reflects the saturation effect in our risk estimation: wind speed is converted to blade tip speed, which plateaus at rated speed of the wind turbine. As a result, further increases in wind speed do not significantly elevate risk. Conversely, in summer, the northeastern offshore region shows high erosion risk despite lower wind speeds, underscoring the dominant role of precipitation in driving seasonal risk variability using this metric.

These seasonal and spatial variations support the importance of site-specific mitigation strategies for turbine blade erosion, such as selecting advanced coatings (e.g., graphene-enhanced or superhydrophobic

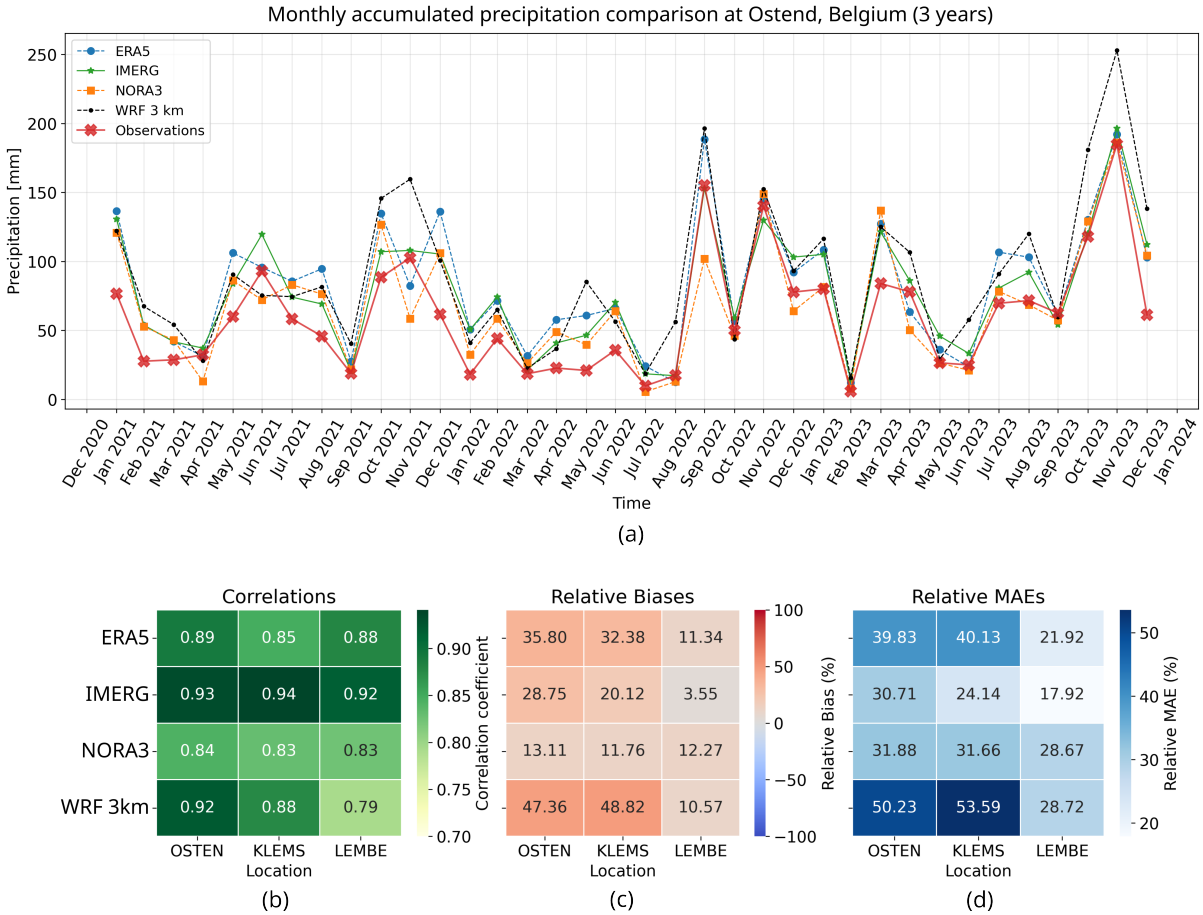

Figure 3: Comparison of ERA5 reanalysis, IMERG satellite-based estimates, NORA3 hindcast archive, and WRF model output against weather station precipitation data. Monthly accumulated precipitation over three years in Ostend, Belgium (a). Correlation coefficients (b), relative biases (c), and relative mean absolute errors (d) computed for three Belgian weather station locations (which are described in Table 1).

materials). The high-resolution WRF output offers valuable insights into localized precipitation conditions, which can help optimize the selection of erosion-resistant materials and protective coatings based on regional weather characteristics.

5 Conclusions

This study examined precipitation conditions across offshore wind farms in Europe, with a particular focus on the Southern Bight of the North Sea. Using ten years of data from ERA5, IMERG, and three years of high-resolution WRF simulations, we analyzed seasonal and spatial variations in precipitation conditions and provided an indicative map for LEE risks based on hourly precipitation amount and blade tip speed. Our findings highlight regions with pronounced LEE risks in active offshore development zones. A comparison of ERA5, IMERG, NORA3, and WRF with Belgian weather station observations helped evaluate the performance of these datasets in capturing precipitation trends. While ERA5, IMERG, NORA3, and WRF effectively capture monthly precipitation trends, all three datasets exhibit a consistent positive bias when compared to three Belgian weather stations. Despite its higher relative errors, WRF offers valuable insights into local-scale variations. Particularly, WRF revealed substantial spatial heterogeneity in precipitation, which demonstrated that neighboring wind farms experience distinct erosion risks that vary seasonally, despite being relatively closely located.

A few limitations must be acknowledged. Although WRF captures small-scale variability, its accuracy is limited by model parameterizations and uncertainties in input data. This study does not explicitly

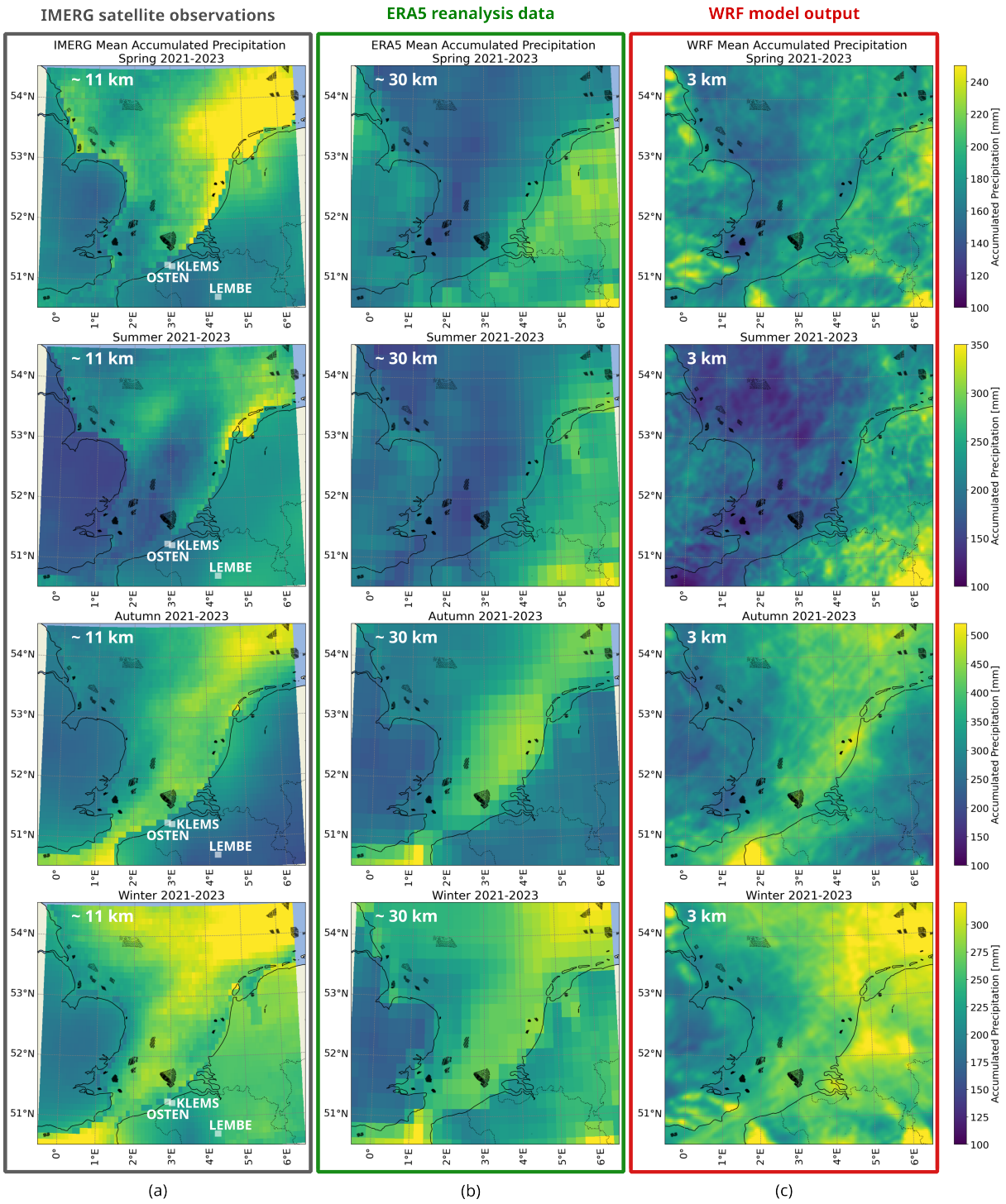

Figure 4: Seasonal precipitation maps for the Southern Bight of the North Sea: (a) IMERG satellite-based observations (∼ 11 km grid), (b) ERA5 reanalysis (∼ 30 km grid), and (c) WRF simulation (dynamical downscaling of ERA5 on a 3 km grid).

simulate erosion processes or material degradation. Furthermore, the three-year WRF simulation period may not fully capture inter-annual variability. Extending the WRF simulation period, refining microphysics and cumulus parameterizations, and integrating wind farm effects will enhance the precision of

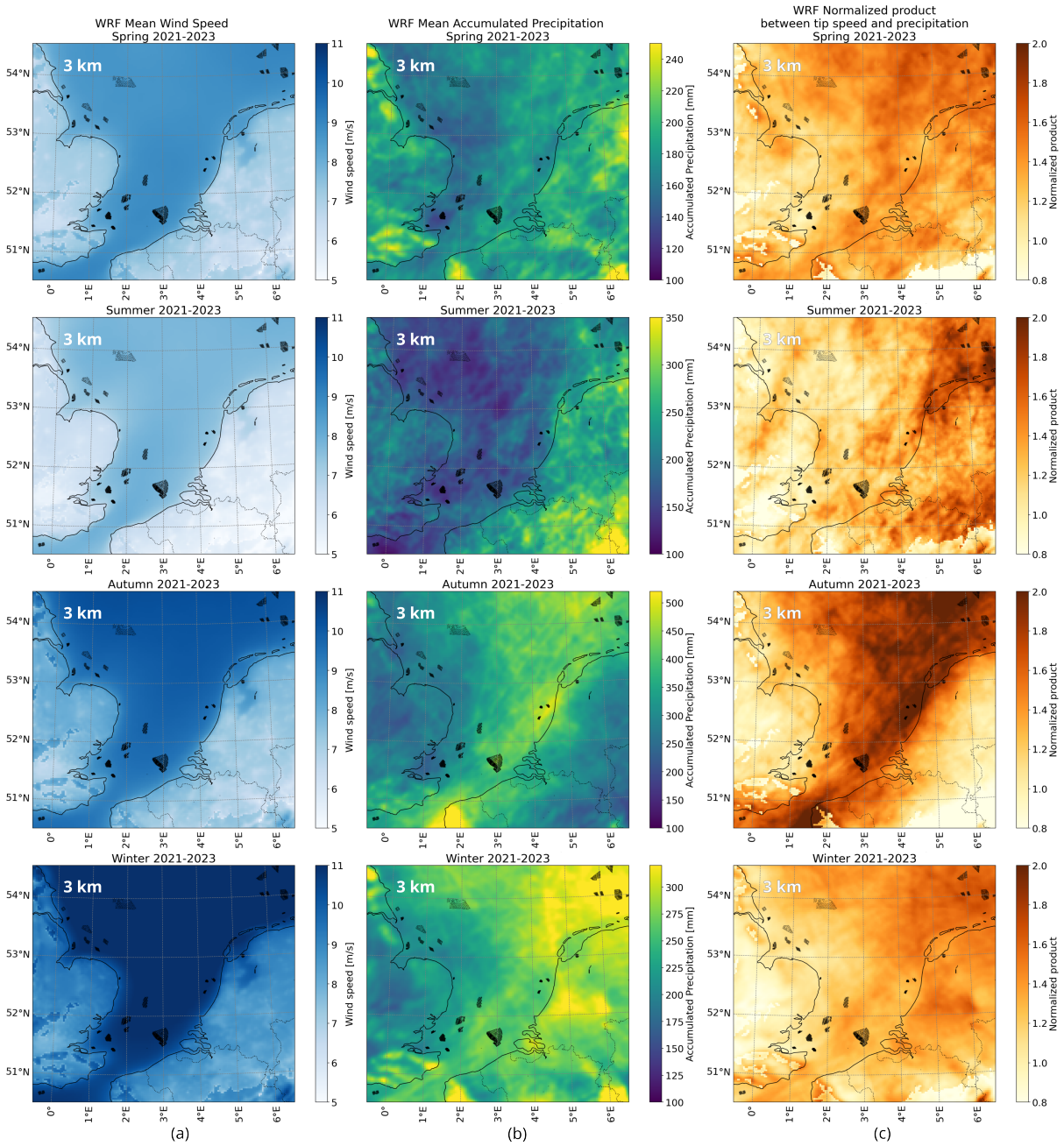

Figure 5: WRF results: (a) seasonal mean wind speed, (b) total accumulated precipitation per season, and (c) the LEE risk indicator, computed from hourly precipitation and blade tip speed.

these weather assessments in future works.

By integrating multiple data sources, this study offers a detailed characterization of the environmental conditions that affect wind turbine longevity and rain-induced erosion risks. This is valuable for early-stage wind farm site screening, informed material selection for blade coatings, and strategic maintenance planning. Future work will focus on extreme precipitation and hail events at a finer temporal granularity, as well as the implementation of advanced LEE models, further supporting efforts for the cost-effectiveness of wind energy projects.

Acknowledgements
The authors acknowledge the BeFORECAST project, supported by the Energy Transition Fund of the Belgian Federal Government, as well as the RS4OWE project, funded by Flanders Innovation & Entrepreneurship (VLAIO). Additionally, they thank the Flemish government for providing open-access weather observations in Belgium (Vlaanderen Waterinfo and Meetnet Vlaamse Banken).

This study relies on open-access data (NASA's IMERG, ECMWF's ERA5, and NORA3), as well as on the open-source WRF code used for conducting the simulations, and various open-source tools and Python libraries used for the post-processing framework. The authors gratefully acknowledge the communities that develop and maintain these valuable resources.

References

[1] Sareen A, Sapre CA, Selig MS. Effects of leading edge erosion on wind turbine blade performance. Wind Energy. 2013 Jul;17(10):1531–1542. Available from: http://dx.doi.org/10.1002/we.1649.

[2] Herring R, Dyer K, Martin F, Ward C. The increasing importance of leading edge erosion and a review of existing protection solutions. Renewable and Sustainable Energy Reviews. 2019 Nov;115:109382. Available from: http://dx.doi.org/10.1016/j.rser.2019.109382.

[3] Bech JI, Hasager CB, Bak C. Extending the life of wind turbine blade leading edges by reducing the tip speed during extreme precipitation events. Wind Energy Science. 2018 Oct;3(2):729–748. Available from: http://dx.doi.org/10.5194/wes-3-729-2018.

[4] Mishnaevsky L, Hasager CB, Bak C, Tilg AM, Bech JI, Doagou Rad S, et al. Leading edge erosion of wind turbine blades: Understanding, prevention and protection. Renewable Energy. 2021 May;169:953–969. Available from: http://dx.doi.org/10.1016/j.renene.2021.01.044.

[5] Hasager CB, Vejen F, Skrzypiński WR, Tilg AM. Rain Erosion Load and Its Effect on Leading-Edge Lifetime and Potential of Erosion-Safe Mode at Wind Turbines in the North Sea and Baltic Sea. Energies. 2021 Apr;14(7):1959. Available from: http://dx.doi.org/10.3390/en14071959.

[6] Hasager C, Vejen F, Bech JI, Skrzypiński WR, Tilg AM, Nielsen M. Assessment of the rain and wind climate with focus on wind turbine blade leading edge erosion rate and expected lifetime in Danish Seas. Renewable Energy. 2020 Apr;149:91–102. Available from: http://dx.doi.org/10.1016/j.renene.2019.12.043.

[7] Letson F, Barthelmie RJ, Pryor SC. Radar-derived precipitation climatology for wind turbine blade leading edge erosion. Wind Energy Science. 2020 Mar;5(1):331–347. Available from: http://dx.doi.org/10.5194/wes-5-331-2020.

[8] Herring R, Dyer K, Howkins P, Ward C. Characterisation of the offshore precipitation environment to help combat leading edge erosion of wind turbine blades. Wind Energy Science. 2020 Oct;5(4):1399–1409. Available from: http://dx.doi.org/10.5194/wes-5-1399-2020.

[9] Letson F, Shepherd TJ, Barthelmie RJ, Pryor SC. WRF Modeling of Deep Convection and Hail for Wind Power Applications. Journal of Applied Meteorology and Climatology. 2020 Oct;59(10):1717–1733. Available from: http://dx.doi.org/10.1175/JAMC-D-20-0033.1.

[10] Pugh K, Stack MM. Rain Erosion Maps for Wind Turbines Based on Geographical Locations: A Case Study in Ireland and Britain. Journal of Bio- and Tribo-Corrosion. 2021 3;7.

[11] Badger M, Zuo H, Hannesdóttir Á, Owda A, Hasager C. Lifetime prediction of turbine blades using global precipitation products from satellites. Wind Energy Science. 2022 Dec;7(6):2497–2512. Available from: http://dx.doi.org/10.5194/wes-7-2497-2022.

[12] Pryor SC, Barthelmie RJ, Cadence J, Dellwik E, Hasager CB, Kral ST, et al. Atmospheric Drivers of Wind Turbine Blade Leading Edge Erosion: Review and Recommendations for Future Research. Energies. 2022 Nov;15(22):8553. Available from: http://dx.doi.org/10.3390/en15228553.

[13] Visbech J, Göçmen T, Hasager CB, Shkalov H, Handberg M, Nielsen KP. Introducing a data-driven approach to predict site-specific leading-edge erosion from mesoscale weather simulations. Wind Energy Science. 2023 Feb;8(2):173–191. Available from: http://dx.doi.org/10.5194/wes-8-173-2023.

[14] Hannesdóttir Á, Kral ST, Reuder J, Hasager CB. Rain erosion atlas for wind turbine blades based on ERA5 and NORA3 for Scandinavia. Results in Engineering. 2024 Jun;22:102010. Available from: http://dx.doi.org/10.1016/j.rineng.2024.102010.

[15] Hannesdóttir Á, Dellwik E, Hasager CB. Prediction of rain erosion damage progression using disdrometer rain data: The importance of liquid water content. Journal of Physics: Conference Series. 2024 Jun;2767(4):042024. Available from: http://dx.doi.org/10.1088/1742-6596/2767/4/042024.

[16] Caboni M, Slot HM, Bergman G, Wouters DAJ, Van Der Mijle Meijer HJ. Evaluation of wind turbine blades' rain-induced leading edge erosion using rainfall measurements at offshore, coastal and onshore locations in the Netherlands. Journal of Physics: Conference Series. 2024 Jun;2767(6):062003. Available from: http://dx.doi.org/10.1088/1742-6596/2767/6/062003.

[17] Caboni M, van Dalum G. Developing an atlas of rain-induced leading edge erosion for wind turbine blades in the Dutch North Sea. Preprint under review for Wind Energy Science. 2024 Dec. Available from: http://dx.doi.org/10.5194/wes-2024-174.

[18] Dimitriadou K, Hasager CB, Nouqueret EC, Hannesdóttir Á. Quality assessment of the GPM IMERG product for lifetime prediction of turbine blades in complex terrain. Journal of Physics: Conference Series. 2024 Jun;2767(4):042010. Available from: http://dx.doi.org/10.1088/1742-6596/2767/4/042010.

[19] Hersbach H, Bell B, Berrisford P, Biavati G, Horányi A, Muñoz Sabater J, et al. ERA5 hourly data on single levels from 1940 to present. Copernicus Climate Change Service (C3S) Climate Data Store (CDS); 2018. (Last accessed: 5 March 2025).

[20] Huffman G, Bolvin D, Joyce R, Kelley O, Nelkin E, Tan J, et al. Integrated Multi-satellitE Retrievals for GPM (IMERG), version 7, Technical Documentation. NASA; 2023. (Last accessed: 5 March 2025). Available from: https://gpm.nasa.gov/data/imerg.

[21] Huffman GJ, Stocker EF, Bolvin DT, Nelkin EJ, Jackson T. NASA, editor. GPM IMERG Final Precipitation L3 1 day 0.1 degree x 0.1 degree V07. NASA Goddard Earth Sciences Data and Information Services Center; 2023. Precipitation Processing System (PPS) At NASA GSFC (Last accessed: 5 March 2025). Available from: https://disc.gsfc.nasa.gov/datasets/GPM_3IMERGDF_07/summary.

[22] Skamarock WC, Klemp JB. A time-split nonhydrostatic atmospheric model for weather research and forecasting applications. Journal of Computational Physics. 2008 Mar;227(7):3465–3485. Available from: http://dx.doi.org/10.1016/j.jcp.2007.01.037.

[23] Skamarock WC, Klemp JB, Dudhia J, Gill DO, Liu Z, Berner J, et al. A Description of the Advanced Research WRF Model Version 4.3. UCAR/NCAR; 2019. (Last accessed: 5 March 2025). Available from: https://opensky.ucar.edu/islandora/object/opensky:2898.

[24] Agency for Maritime Services and Coast. Precipitation Measurements. Meetnet Vlaamse Banken; 2025. (Last accessed: 5 March 2025). Available from: https://meetnetvlaamsebanken.be/.

[25] Vlaanderen Waterinfo. Precipitation Measurements. Flemish Government; 2025. (Last accessed: 5 March 2025). Available from: https://www.waterinfo.be/Themas.

[26] Haakenstad H, Breivik Ø, Furevik BR, Reistad M, Bohlinger P, Aarnes OJ. NORA3: A Nonhydrostatic High-Resolution Hindcast of the North Sea, the Norwegian Sea, and the Barents Sea. Journal of Applied Meteorology and Climatology. 2021 Oct;60(10):1443–1464. Available from: http://dx.doi.org/10.1175/JAMC-D-21-0029.1.

[27] Haakenstad H, Breivik Ø. NORA3. Part II: Precipitation and Temperature Statistics in Complex Terrain Modeled with a Nonhydrostatic Model. Journal of Applied Meteorology and Climatology. 2022 Oct;61(10):1549–1572. Available from: http://dx.doi.org/10.1175/JAMC-D-22-0005.1.

[28] Hoeser T, Feuerstein S, Kuenzer C. DeepOWT: a global offshore wind turbine data set derived with deep learning from Sentinel-1 data. Earth System Science Data. 2022 Sep;14(9):4251–4270. Available from: http://dx.doi.org/10.5194/essd-14-4251-2022.

[29] Hoeser T, Kuenzer C. DeepOWT: A global offshore wind turbine data set. Zenodo; 2022. (Last accessed: 5 March 2025). Available from: https://zenodo.org/record/5933967.

[30] Kainz S, Quick J, Souza de Alencar M, Sanchez Perez Moreno S, Dykes K, Bay CJ, et al. The IEA Wind 740-10-MW Reference Offshore Wind Plants, IEA Wind Task 55. NREL Tech. Rep.; 2024. (Last accessed: 5 March 2025). Available from: https://www.nrel.gov/docs/fy24osti/87923.pdf.

[31] Derin Y, Kirstetter PE, Brauer N, Gourley JJ, Wang J. Evaluation of IMERG Satellite Precipitation over the Land–Coast–Ocean Continuum. Part II: Quantification. Journal of Hydrometeorology. 2022 Aug;23(8):1297–1314. Available from: http://dx.doi.org/10.1175/JHM-D-21-0234.1.

[32] Palatos-Plexidas A, De Paepe G, Bonnefoy L, Gremmo S, Van Beeck J, De Cruz L, et al. Identifying Wake Patterns in Weather Regimes over the Southern Bight of the North Sea using clustering techniques. Journal of Physics: Conference Series. 2025 May;3016(1):012046. Available from: http://dx.doi.org/10.1088/1742-6596/3016/1/012046.

[33] Hahmann AN, Sile T, Witha B, Davis NN, Dörenkämper M, Ezber Y, et al. The making of the New European Wind Atlas - Part 1: Model sensitivity. Geoscientific Model Development. 2020 10;13:5053-78.

[34] Dörenkämper M, Olsen BT, Witha B, Hahmann AN, Davis NN, Barcons J, et al. The Making of the New European Wind Atlas - Part 2: Production and evaluation. Geoscientific Model Development. 2020 10;13:5079-102.

[35] Lee JCY, Lundquist JK. Evaluation of the wind farm parameterization in the Weather Research and Forecasting model (version 3.8.1) with meteorological and turbine power data. Geoscientific Model Development. 2017 Nov;10(11):4229-44. Available from: https://doi.org/10.5194/gmd-10-4229-2017.

[36] Yang B, Zhong L, Wang J, Shu H, Zhang X, Yu T, et al. State-of-the-art one-stop handbook on wind forecasting technologies: An overview of classifications, methodologies, and analysis. Journal of Cleaner Production. 2021 Feb;283:124628. Available from: https://doi.org/10.1016/j.jclepro.2020.124628.